Journal of Magnetic Resonance **142,** 229–240 (2000)
doi:10.1006/jmre.1999.1876, available online at http://www.idealibrary.com on IDEAL®

Characterization of Molecular Motion in the Solid State by Carbon-13 Spin–Lattice Relaxation Times

Samuel J. Varner, Robert L. Vold,*[,1] and Gina L. Hoatson

*Department of Physics and *Department of Applied Science, College of William and Mary, P.O. Box 8795, Williamsburg, Virginia 23187-8795*

Received March 12, 1999; revised July 6, 1999

Relaxation calculations for rapidly spinning samples show that spin–lattice relaxation time (T_{1Z}) anisotropy varies with the angle between the rotor spinning axis and the external field. When the rate of molecular motion is in the extreme narrowing limit, the measurement of T_{1Z} anisotropies for two different values of the spinning angle allows the determination of two linear combinations of the three static spectral densities, $J_0(0)$, $J_1(0)$, and $J_2(0)$. These functions are sensitive to molecular geometry and the rate and trajectory of motion. The utility of these linear combinations in the investigation of molecular dynamics in solids has been demonstrated with natural abundance ^{13}C NMR experiments on ferrocene. In an isolated ^{13}C–^{1,2}H group, the dipole–dipole interaction has the same orientational dependence as the quadrupole interaction. Thus, the spectral densities that are responsible for dipolar relaxation of ^{13}C are the same as those responsible for deuteron quadrupolar relaxation. For ferrocene-d_{10}, deuteron T_{1Z} and T_{1Q} anisotropies and the relaxation time of the ^{13}C magic angle spinning peak provide sufficient information to determine the orientation dependence of all three individual spectral densities.

Key Words: **carbon; ferrocene; motion; relaxation; anisotropy.**

INTRODUCTION

Measurements of deuteron spin–lattice relaxation times in solids provide detailed information about the rates and trajectories of molecular motion (*1*). This method is especially powerful because the wide powder patterns that result from inhomogeneous broadening by the quadrupolar interaction facilitate measurements of the orientation dependence (anisotropy) of the relaxation times. Moreover, the orientation dependence of individual spectral densities can be determined from measurements of the deuteron relaxation times of Zeeman order, T_{1Z}, and quadrupolar order, T_{1Q} (*1*). Here, we consider the possibility of devising an appropriate set of natural abundance ^{13}C relaxation experiments to provide the same level of detailed motional information as that available from deuteron relaxation studies.

For some systems carbon and deuteron relaxation data are complimentary. The dipolar interaction which dominates ^{13}C relaxation in a ^{13}C–^{1}H group is axially symmetric. Vibrational averaging can lead to an asymmetric averaged tensor; however, this effect is typically small. Quadrupole tensors for ^{13}C–^{2}H groups are also very nearly symmetric. The dipolar and quadrupolar tensors have their largest components oriented along the ^{13}C–^{1,2}H bond. Since these tensors have the same orientations and nearly the same symmetry, they yield magnetic fluctuations with the same frequency components when the internuclear vector changes orientation. Thus, for an isolated ^{13}C–^{1,2}H group, the spectral density anisotropies of the carbon and deuteron are identical.

Quantitative determination of motion by ^{13}C nuclear spin–lattice relaxation time anisotropy presents some challenges. Static ^{13}C spectra consist of chemical shift anisotropy (CSA) powder patterns. When more than one chemically and magnetically distinct ^{13}C nucleus is present in the sample, the overlap of powder patterns often prevents the unambiguous measurement of the orientation dependence of T_{1Z}. Magic angle spinning (MAS) is routinely used to improve the resolution of solid-state ^{13}C NMR spectra. However, since the powder patterns are coherently averaged to give sharp lines at the isotropic chemical shifts, they contain no orientational information. While isotopic enrichment could be used to produce spectra dominated by one powder pattern, intermolecular ^{13}C–^{13}C spin diffusion would likely equalize relaxation times, destroying the desired anisotropy. Two-dimensional (2D) techniques such as PHORMAT (*2*) or VACSY (*3*) provide CSA powder patterns, separated in the second dimension on the basis of isotropic chemical shift. If such a 2D pulse sequence is preceded by an inversion pulse and variable relaxation delay, the resulting set of partially relaxed 2D spectra may provide some information about orientation-dependent relaxation times. A later section of this paper considers how the experimental conditions imposed by such experiments influence the observed relaxation time anisotropy.

A second problem is that a large number spectral densities can contribute to carbon relaxation. For deuterons, only two spectral densities from the autocorrelation of the quadrupole interaction are important. For carbon relaxation, spectral densities that arise from auto- and cross-correlations of chemical

[1] To whom correspondence should be addressed. E-mail: rlv@as.wm.edu. Fax: (757) 221-3540.

1090-7807/00 $35.00

shielding anisotropy, spin rotation, and dipolar couplings may need to be considered. Even for the simple case of an isolated ^{13}C–^{1}H spin pair relaxed only by a time-dependent dipole–dipole coupling, three spectral densities must be determined. For more complex carbon–proton spin systems significant additional spectral densities arise from cross-correlation or interference between different pairwise dipolar interactions (*4*). For many motional processes, the anisotropies of different spectral densities have the opposite sense and consequently the corresponding relaxation times show a reduced dependence on orientation. It is therefore important to measure as many different linear combinations of spectral densities as possible. Ideally, enough independent measurements should be made to permit determination of the anisotropy of each individual spectral density. In liquids, significant progress has been made toward this goal by designing selective excitation pulse sequences to prepare the spins in appropriate initial states (*4–7*). However, solid samples are far more challenging because extensive dipolar coupling and line broadening complicate such selective excitation (*8*).

In this paper, expressions for the fast limit spectral densities of spinning samples are derived. These expressions are used to show how two independent linear combinations of the spectral densities may be determined. In addition, a method is presented for measuring all three spectral density anisotropies independently, using the deuteron T_{1Z} and T_{1Q} anisotropies and the ^{13}C MAS T_{1Z}. Experimentally determined linear combinations of ^{13}C spectral densities are presented for unlabeled ferrocene. Finally, the orientation dependence of the three individual spectral densities, determined by conducting experiments on natural abundance ^{13}C and deuterated ferrocene, is shown.

CALCULATIONS

In the extreme narrowing limit, for relaxation dominated by the dipole–dipole mechanism, the ^{13}C Zeeman relaxation rate is given by a linear combination of spectral densities (*9*),

$$R_{1Z} = \frac{1}{T_{1Z}} = \frac{N\omega_D^2}{2}\left[J_0(\omega_I - \omega_S) + 3J_1(\omega_I) + 6J_2(\omega_I + \omega_S)\right], \quad [1]$$

where N is the number of I spins (protons, in this case) directly bonded to the relaxing S spin (carbon), and $\omega_D = \gamma_I\gamma_S\hbar\langle 1/r_{IS}^3\rangle$, the dipolar coupling. The angular brackets indicate that the factor $1/r_{IS}^3$ is averaged over vibrational motions which are too fast to contribute appreciably to the spectral densities. Cross-correlation between different ^{13}C–^{1}H vectors is ignored in this calculation.

For deuterons, relaxation is induced by fluctuations in the quadrupole interaction. In this case the relaxation rate of Zeeman order is given by (*10*)

$$R_{1Z} = \frac{3\pi^2}{2}\chi^2[J_1(\omega_0) + 4J_2(2\omega_0)], \quad [2]$$

where $\chi = e^2q_{zz}Q/h$ is the quadrupole coupling constant. Here, e is the electronic charge, q_{zz} is the largest principal component of the electric field gradient tensor, and Q is the quadrupole moment of the deuteron. As with the dipolar coupling constant, the quadrupole coupling constant is averaged over fast vibrations. Relaxation of quadrupolar order is described by a single spectral density,

$$R_{1Q} = \frac{9\pi^2}{2}\chi^2 J_1(\omega_0). \quad [3]$$

The normalized spectral densities are defined as Fourier transforms of the autocorrelation functions,

$$J_m(\omega) = \frac{1}{[T_0^{(2)}(\mathrm{PAS})]^2}\int_0^\infty \langle T_m^{(2)}(\mathrm{LAB}, t) \times T_m^{(2)*}(\mathrm{LAB}, t+\tau)\rangle e^{-im\omega\tau}d\tau, \quad [4]$$

where $T_m^{(2)}$ (LAB) is the relevant interaction tensor in the laboratory coordinate system. This tensor is found by a transformation of coordinate systems from the principal axis system (PAS), where the tensor is diagonal, to the laboratory coordinate system through the Euler angles $\Omega_{PL} = (\alpha_{PL}, \beta_{PL}, \gamma_{PL})$.

Spectral Densities of Spinning Samples

In this section, Eq. [4] is evaluated to determine the spectral densities in a spinning sample. The transformation from PAS to LAB is performed as a series of rotations involving three intermediate coordinate systems: the molecule-fixed coordinate system (MOL), the crystal-fixed coordinate system (CRYS), and the rotor-fixed coordinate system (ROT). Breaking up the transformations this way separates the time-dependent and time-independent transformations. The successive transformations of the coordinate system from PAS to LAB may be summarized as

$$\mathrm{PAS} \xrightarrow{\Omega_{PM}} \mathrm{MOL} \xrightarrow{\Omega_{MC}(t)} \mathrm{CRYS} \xrightarrow{\Omega_{CR}} \mathrm{ROT} \xrightarrow{\Omega_{RL}(t)} \mathrm{LAB}.$$

The PAS is fixed in the molecule, so the PAS to MOL trans-

formation, Ω_{PM}, is time independent. The CRYS to ROT transformation, Ω_{CR}, is also time independent since the sample is stationary with respect to the rotor. The time dependence of the system is contained in the remaining transformations. The spinning rotor leads to a coherently time-dependent ROT to LAB transformation, $\Omega_{RL}(t) = (\alpha_{RL}(t), \beta_{RL}, \gamma_{RL}))$, while random molecular motion is responsible for the time dependence of the MOL to CRYS rotation, $\Omega_{MC} = (\alpha_{MC}(t), \beta_{MC}(t), \gamma_{MC}(t))$. The transformation $\Omega_{MC}(t)$ is of particular importance since its time dependence describes the fluctuating local magnetic fields that induce relaxation.

For spherical irreducible tensors, the successive transformations that take the dipolar tensor from PAS to LAB are performed by summing over Wigner rotation matrix elements. Thus, the spectral densities are written

$$J_m(\omega) = \frac{1}{[T_0^{(2)}(\mathrm{PAS})]^2} \sum_{a,a'=-2}^{2} \sum_{b,b'=-2}^{2} \sum_{c,c'=-2}^{2} \sum_{d,d'=-2}^{2} \int_0^\infty \langle D_{am}^{(2)}(\Omega_{RL}(t))\, D_{a'm}^{(2)*}(\Omega_{RL}(t+\tau))\, D_{ba}^{(2)}(\Omega_{CR}(t))\, D_{b'a'}^{(2)*}(\Omega_{CR}(t+\tau))\, D_{cb}^{(2)}(\Omega_{MC}(t))\, D_{c'b'}^{(2)*}(\Omega_{MC}(t+\tau))\, D_{dc}^{(2)}(\Omega_{PM}(t))\, D_{d'c'}^{(2)*}(\Omega_{PM}(t+\tau))\, T_d^{(2)}(\mathrm{PAS}) T_{d'}^{(2)*}(\mathrm{PAS})\rangle e^{-im\omega\tau} d\tau. \quad [5]$$

Since the dipolar tensor is a second-rank tensor interaction, all summations over Wigner matrix elements will be from -2 to 2. These limits will be omitted in subsequent equations.

Several assumptions can be made to simplify Eq. [5]. For the axially symmetric dipolar interaction, only the $T_0^{(2)}$ (PAS) component is nonzero. Two of the transformations are time independent so the corresponding Wigner matrix elements may be removed from the integral. Also, since molecular motion is a stationary Markov process, the time t can be set to zero without loss of generality. With these modifications the spectral densities become

$$J_m(\omega) = \sum_{a,a'} \sum_{b,b'} \sum_{c,c'} D_{ba}^{(2)}(\Omega_{CR})\, D_{b'a'}^{(2)*}(\Omega_{CR}) \times D_{0c}^{(2)}(\Omega_{PM})\, D_{0c'}^{(2)*}(\Omega_{PM}) \int_0^\infty \langle D_{am}^{(2)}(\Omega_{RL}(0))\, D_{a'm}^{(2)*}(\Omega_{RL}(\tau))\, D_{cb}^{(2)}(\Omega_{MC}(0))\, D_{c'b'}^{(2)*}(\Omega_{MC}(\tau))\rangle e^{-i\omega\tau} d\tau. \quad [6]$$

For most physically reasonable situations the equations may be further simplified by recognizing that the rotor period is long compared to the correlation time but short compared to typical ^{13}C relaxation times. Correlation times are generally on the order of picoseconds, and rotor periods are typically tenths of milliseconds. Thus, the rotor may be considered stationary for the time period in which the integrand is nonzero. This fast motion approximation allows the Wigner matrix elements for the Ω_{RL} transformation to be taken outside of the integral. Carbon relaxation times are generally longer than a few seconds; while the nuclei relax, the rotor undergoes thousands of rotations. Thus, the relaxation times depend on spectral densities averaged over a rotor cycle. For this situation the ROT to LAB transformation is determined completely by the angle between the rotor axis and the external field, β_{RL}. Thus, the following identity is valid:

$$\langle D_{am}^{(2)}(\Omega_{RL}(0))\, D_{a'm}^{(2)*}(\Omega_{RL}(\tau))\rangle = |d_{am}^{(2)}(\beta_{RL})|^2 \delta_{a,a'}. \quad [7]$$

Assuming uniaxial motion about the molecule-fixed axis, the MOL to CRYS transformation is reduced to a simple rotation about that axis. For this this type of motion, the expression for the spectral densities is simplified since

$$\langle D_{cb}^{(2)}(\Omega_{MC}(0))\, D_{c'b'}^{(2)*}(\Omega_{MC}(\tau))\rangle = \langle e^{-ib\alpha_{MC}(0)} e^{ib'\alpha_{MC}(\tau)}\rangle \delta_{b,c}\delta_{b',c'}. \quad [8]$$

Torchia and Szabo (*9*) denote correlation function of the MOL to CRYS transformation by

$$\Gamma_{b,b'}(\tau) = \langle e^{-ib\alpha_{MC}(0)} e^{ib'\alpha_{MC}(\tau)}\rangle. \quad [9]$$

This function has been evaluated for a variety of axial motional models in Ref. (*9*).

Making these assumptions, the expression for the spectral densities in a spinning sample can now be written as

$$J_m(\omega) = \sum_a \sum_{b,b'} |d_{am}^{(2)}(\beta_{RL})|^2 D_{ba}^{(2)}(\Omega_{CR})\, D_{b'a}^{(2)*}(\Omega_{CR})\, D_{0b}^{(2)}(\Omega_{PM})\, D_{0b'}^{(2)*}(\Omega_{PM}) \int_0^\infty \Gamma_{b,b'}(\tau) e^{-im\omega\tau} d\tau. \quad [10]$$

For jump models with five or more equally populated sites, $\Gamma_{b,b'}$ is diagonal (*9*), and the spectral densities become

$$J_m(\omega) = \sum_{a,b} |d_{am}^{(2)}(\beta_{RL})|^2 |d_{ba}^{(2)}(\beta_{CR})|^2 |d_{0b}^{(2)} \times (\beta_{PM})|^2 \int_0^\infty \Gamma_{b,b}(\tau) e^{-im\omega\tau} d\tau. \quad [11]$$

For this study, Eq. [11] has been evaluated numerically for a

variety of molecular geometries and models of molecular motion. Relaxation time anisotropies calculated from these spectral densities were studied and compared to measurements of ferrocene.

Comparison to Static Spectral Densities

In the fast motion limit, the spectral densities for a spinning sample depend on a number of time-independent transformations. For the PAS to MOL transformation, β_{PM} is fixed by molecular geometry. The spinning angle, β_{RL}, can be adjusted in the probe. However, for a powder sample, each crystallite has a pair of angles (β_{CR} and γ_{CR}) that describe the CRYS to ROT transformation. These angles determine the position of a crystallite's spectral line in the CSA powder pattern of a spinning sample. For a static sample the rotor frame is omitted from the transformations. Thus, for arbitrary correlation functions, $\Gamma_{b,b'}(\tau)$ (*9*), the expression for the static spectral densities is

$$J'_m(\omega) = \sum_a \sum_{b,b'} D^{(2)}_{ba}(\Omega_{CL})\, D^{(2)*}_{b'a}(\Omega_{CL})\, D^{(2)}_{0b}(\Omega_{PM})\, D^{(2)*}_{0b'}(\Omega_{PM}) \int_0^\infty \Gamma_{b,b'}(\tau) e^{-im\omega\tau} d\tau. \quad [12]$$

If the ROT to LAB transformation is omitted from Eq. [10] then the expression for the spinning spectral densities resembles that for the static case. The only difference is that the Euler angle Ω_{CR} appears instead of Ω_{CL} when the sample is spinning. In a static sample, the spectral frequency depends on Ω_{CL} in the same way as the frequency in a spinning sample depends on Ω_{CR}. The relationship between $J_m(\omega)$ and $J'_m(\omega)$ is expressed simply if orientation rather than chemical shift is used to identify a point on a lineshape,

$$J_m(\omega, \beta_{CR}) = \sum_a |d^{(2)}_{am}(\beta_{RL})|^2 J'_a(\omega, \beta_{CL}). \quad [13]$$

This expression shows that for each point on the lineshape of a spinning sample the spectral densities are linear combinations of the spectral densities for the corresponding point on the static lineshape.

The frequency for crystallites oriented at some particular value of β_{CR} is the same as that for $180° \pm \beta_{CR}$ and $360° - \beta_{CR}$. In general, spectral densities do not have such high symmetry. Two values of β_{CR} that give the same spectral frequency may yield different spectral densities. If this is the case then relaxation is multiexponential.

Linear Combinations of Spectral Densities

If the motional rate (jump rate or diffusion coefficient) is much higher than the relevant combination of Larmor frequencies, the spectral densities are effectively independent of frequency, $J_m(\omega) \approx J_m(0)$. When this extreme narrowing condition is met, the spinning spectral densities can be written in terms of their static counterparts, $J'_0(0)$, $J'_1(0)$, and $J'_2(0)$. In this case, the expression for R_{1Z} in a spinning sample can be written in terms of the static spectral densities and the spinning angle,

$$R_{1Z}(\beta_{RL}) = \frac{N\omega_D^2}{2}\left[\frac{1}{2}(5 - 3\cos^2(\beta_{RL}))J'_0(0) + \frac{1}{2}(9 - 3\cos^2(\beta_{RL}))J'_1(0) + 3(1 + \cos^2(\beta_{RL}))J'_2(0)\right]. \quad [14]$$

Thus, the relaxation rate is a linear combination of the static spectral densities with coefficients determined by the spinning angle. This suggests a method for determining the static spectral densities from spinning relaxation time anisotropies. By measuring relaxation time anisotropies for a variety of spinning angles a set of equations could be constructed and solved to give the static spectral densities. However, rearranging Eq. [14] yields a term that depends on the spinning angle and a constant term,

$$R_{1Z}(\beta_{RL}) = \frac{N\omega_D^2}{2}[A + B\cos^2(\beta_{RL})] \quad [15]$$

where

$$A = \frac{5}{2}J'_0(0) + \frac{9}{2}J'_1(0) + 3J'_2(0) \quad [16]$$

and

$$B = -\frac{3}{2}J'_0(0) - \frac{3}{2}J'_1(0) + 3J'_2(0). \quad [17]$$

Thus, only two linearly independent combinations of the static spectral densities can be determined from experiments performed with a variety of spinning angles.

These two linear combinations, A and B, are easily determined from experimental data by recognizing that

$$A = R_{1Z}(90°)\frac{2}{N\omega_D^2} \quad [18]$$

and

$$B = (R_{1Z}(0°) - R_{1Z}(90°))\,\frac{2}{N\omega_D^2}. \qquad [19]$$

It is impractical to perform a spinning experiment with $\beta_{RL} = 0°$ since this would place the coil of the probe parallel to the external field and give no signal. However, evaluation of Eq. [13] for $\beta_{RL} = 0°$ shows that, for this case, the spectral densities in a spinning sample are identical to those in a static sample. Thus the linear combinations A and B can be determined by measuring the relaxation time anisotropy in a static sample and a sample spinning about an axis perpendicular to the external field. If there is some overlap of powder patterns in the static spectrum it may be possible to choose a different pair of rotor angles such that the CSA powder patterns are resolved but still wide enough to allow determination of relaxation time anisotropies.

For a sample spun at the magic angle ($\beta_{magic} = \cos^{-1}(1/\sqrt{3})$), powder patterns are collapsed to narrow lines at their isotropic chemical shifts. All crystallite orientations contribute to a frequency range that is narrower than the homogeneous linewidth. Clearly, it is impossible to measure the relaxation of differently oriented crystallites from such a lineshape. If the correlation function, $\Gamma_{b,b'}(t)$, is diagonal there is no relaxation time anisotropy in a sample spinning at the magic angle, and the MAS relaxation time is independent of orientation. Evaluation of Eq. [14] for $\beta_{RL} = \beta_{magic}$ yields

$$R_{1Z} = N\omega_D^2[\,J'_0(0) + 2J'_1(0) + 2J'_2(0)]. \qquad [20]$$

This combination of spectral densities is not linearly independent of A and B, but it is experimentally accessible even for complicated spectra.

The relaxation time of the MAS peak can be used in conjunction with deuteron relaxation times to determine all three spectral densities. Although this strategy requires isotopic labeling for the deuteron experiments it has the advantage that MAS enhances resolution and signal-to-noise ratio in the carbon experiments. It should be stressed that the relaxation time anisotropy vanishes for magic angle spinning only when the correlation function is diagonal, as it is for jump motion with five or more sites equivalent sites or for free rotational diffusion (*9*).

Although carbon dipolar relaxation and deuteron quadrupolar relaxation depend on the same spectral densities (to the extent that they can be treated as axially symmetric), the relaxation rate expressions involve different coupling strengths. The deuteron quadrupole coupling constant may be determined, with reasonable accuracy, from the width of a low-temperature powder pattern. However, determining the dipolar coupling between a ^{13}C nucleus and a nearby proton is not so straightforward. ^{13}C–^{1}H pairs are rarely sufficiently isolated that a dipolar powder pattern can be measured. Since dipolar relaxation rates depend on the sixth power of the internuclear distance, r_{CH}^6, the calculated rates depend sensitively on this value. A recent paper by Hardy *et al.* (*11*) demonstrates that care must be taken when using published bond lengths, since measurements made with different techniques are averaged differently by vibrations of the nuclei. Neutron scattering yields a vibrationally averaged bond length, $\langle r\rangle$. However, the average dipolar coupling, ω_D, is determined by an effective bond length of $\langle 1/r_{CH}^3\rangle^{-1/3}$. In general, these two vibrational averages differ from each other and from the equilibrium bond length, r_e. For typical molecular potentials, $r_e < \langle r\rangle < \langle 1/r_{CH}^3\rangle^{-1/3}$ (*11–13*).

Relaxation Time Anisotropies in Two-Dimensional Experiments

When the overlap of ^{13}C powder patterns prevents accurate measurement of chemical shift anisotropies, 2D techniques can often be used to separate the anisotropic lineshapes. A number of experimental techniques are available for separating CSA powder patterns on the basis of their isotropic chemical shift values (*14*). This suggests that the incorporation of an inversion pulse and a relaxation delay into these experiments would allow the measurement of relaxation time anisotropy of each chemically distinct carbon. However, the effect of sample spinning on relaxation time anisotropy must be kept in mind.

The fact that relaxation time anisotropy depends on spinning angle complicates the measurement of partially relaxed powder patterns with variable angle correlation spectroscopy (VACSY). In a VACSY experiment, the anisotropic chemical shift is scaled by varying the spinning angle. The implicit assumption is that the only difference between the spectra taken at different spinning angles is that the widths of the powder patterns are scaled. For partially relaxed spectra this assumption is not valid. The relaxation time anisotropy in a VACSY powder pattern is not related in any simple way to the anisotropies at each of the various spinning angles. However, for axial motional models, simulations show that the anisotropies for $\beta_{RL} < \beta_{magic}$ offset those for $\beta_{RL} > \beta_{magic}$, yielding virtually no relaxation anisotropy for the set of partially relaxed VACSY powder patterns.

Some 2D experiments are performed with MAS using rotor-synchronized pulses to disrupt the averaging of the chemical shift (*15*). If the sample is spun at the magic angle during the relaxation delays, the measured relaxation anisotropy will reflect the averaging of the spectral densities that occurs with MAS. For many motional trajectories no anisotropy would be observed. Even typical magic angle turning frequencies (about 30 Hz) yield rotor periods that are short compared to most carbon relaxation times. The magic angle hopping experiment (*16*) also suffers from this problem since the rapid 120° jumps also cause averaging of the spectral densities.

For spinning angles other than the magic angle, relaxation

time anisotropies could be measured by storing magnetization along the z-axis and quickly reorienting the rotor for the relaxation delay, after which the spinning axis would be returned to the magic angle and the pulse sequence for measuring the 2D spectrum executed as usual. This technique is compatible with the magic angle flipping 2D experiment (*17*) in which the spinning axis is reoriented to allow evolution under the anisotropic chemical shift. By performing this modified magic angle flipping experiment twice, using different spinning angles during relaxation, two linear combinations of the static spectral densities could be determined for each carbon line in the spectrum. This technique would allow high-fidelity information about molecular motion to be obtained for complex systems.

Properties of Calculated Anisotropies

Some interesting properties of the spectral densities of spinning samples may be found by studying the calculated anisotropies. While the spectral density anisotropies depend strongly on the motional rate, number of sites, and orientation of the dipolar tensor, the calculated relaxation time (T_{1Z}) anisotropies often show little sensitivity to the motional model. To illustrate this, the results of calculations for two motional models are presented in Fig. 1. The first column (Figs. 1a, 1c, and 1e) shows the results for a five-site nearest neighbor jump model with $\beta_{PM} = 90°$. This model is appropriate for ferrocene. The results in the second column are for a three-site model with $\beta_{PM} = 70.5°$, typical of a methyl group.

In both cases, the motion is assumed to be in the extreme narrowing limit. Thus, the CSA powder patterns are axially symmetric with the greatest intensity arising from perpendicularly oriented crystallites, $\beta_{CR} = 90°$. The chemical shielding of this spectral position is denoted $\sigma_\perp$. The weak shoulder of the lineshape is from crystallites that have their z-axes nearly parallel to the rotor axis ($\beta_{CR} \approx 0°$) whose shielding is denoted $\sigma_\parallel$. Although spinning the sample scales the powder pattern by a factor of $d^{(2)}_{00}(\beta_{RL}) = (3\cos^2\beta_{RL} - 1)/2$, corresponding positions on the lineshapes have the same β_{CR} value. Static samples are treated as samples spinning at $\beta_{RL} = 0$ since spinning at this angle has no effect on the spectrum. For this case $\beta_{CR} = \beta_{CL}$. For consistency, the angle that determines the spectral frequency will be called β_{CR} throughout the remainder of this paper. The variable $\sigma = \frac{2}{3}(\sigma_\parallel - \sigma_\perp)d^{(2)}_{00}(\beta_{CR}) + \sigma_{iso}$ is used to denote frequency.

Figures 1a and 1b show that the calculated static spectral densities plotted as a function of σ are quite distinct for these two models. In both cases the spectral densities, like the NMR frequencies, are found to depend only on the angle β_{CR}. The symmetry of the ferrocene spectral densities is such that $J_m(0, \beta_{CR}) = J_m(0, n180° \pm \beta_{CR})$, where $n = 0, 1, 2, \ldots$. Thus, for every frequency on the powder pattern there is a unique set of three spectral densities and a unique relaxation time. However, for the methyl spectral densities, the symmetry relation is $J_m(0, \beta_{CR}) = J_m(0, n180° + \beta_{CR})$. Although crystallites oriented at β_{CR} and $(180° - \beta_{CR})$ have the same NMR frequencies, they have different spectral densities. This implies biexponential relaxation. Even though the individual spectral densities for β_{CR} and $(180° - \beta_{CR})$ are different, the linear combination which determines the relaxation time, T_{1Z}, is the same for both orientations. Thus, in the extreme narrowing limit, the relaxation of each point on a methyl powder pattern is a single exponential function (*9*).

Although the linear combinations, A and B (defined in Eqs. [16] and [17]), are not as distinctive as the individual spectral densities, they do allow these two models to be easily distinguished, as shown in Figs. 1e and 1f. The most notable difference in the anisotropies is seen at the parallel ($\beta_{CR} = 0°$, $\sigma = \sigma_\parallel$) edge of the CSA powder pattern. At this point A and B have the same value for the ferrocene calculations, but are significantly different for the methyl spectrum. As with the T_{1Z} anisotropies, A and B do not depend on the β_{CR} quadrant for either model. While it is unlikely that a relaxation experiment would be needed to distinguish methyl rotation from five-site jumps, the differences in these particular linear combinations of spectral densities highlight an important feature: the degree of separation between A and B at the parallel edge is sensitively dependent on β_{PM}, the angle between the ^{13}C–^{1}H vector and the motional axis.

EXPERIMENTS

Experiments were performed on a homebuilt spectrometer with a Tecmag Libra pulse programmer and a 7-T Oxford superconducting magnet. The Larmor frequency is 75.46 MHz for ^{13}C and 300.07 MHz for ^{1}H. The natural abundance ferrocene sample consisted of 103 mg of the material ground to a fine powder and packed into a 5-mm rotor. A Doty Scientific DSI-313 MAS probe, with a manually variable spinning angle, was used to collect the data presented here. Samples were spun at approximately 4 kHz. The precise values of the angles used in the off magic angle spinning (OMAS) experiments were determined by comparing the widths of the spinning chemical shift powder patterns to the static lineshape. The anisotropic lineshape parameters were determined by a least-squares fitting routine that uses the SUMS powder pattern calculation algorithm (*18*).

For the ^{13}C relaxation experiments, a spin temperature alternation pulse sequence (*19*) was used to produce spectra that decay to zero at long relaxation delays. The cross-polarization (CP) contact time was 1 ms and a recycle delay of 40 s was used to allow for proton relaxation. The proton 90° pulse length was 4 μs. Power in the proton channel was kept constant during cross-polarization and acquisition of the carbon signals, resulting in a decoupling field strength of 63 kHz. The relaxation delays used in the ferrocene T_{1Z} experiments were 0.1, 2, 4, 8, 16, and 32 s. All relaxation experiments were performed at room temperature, 296 ± 2 K.

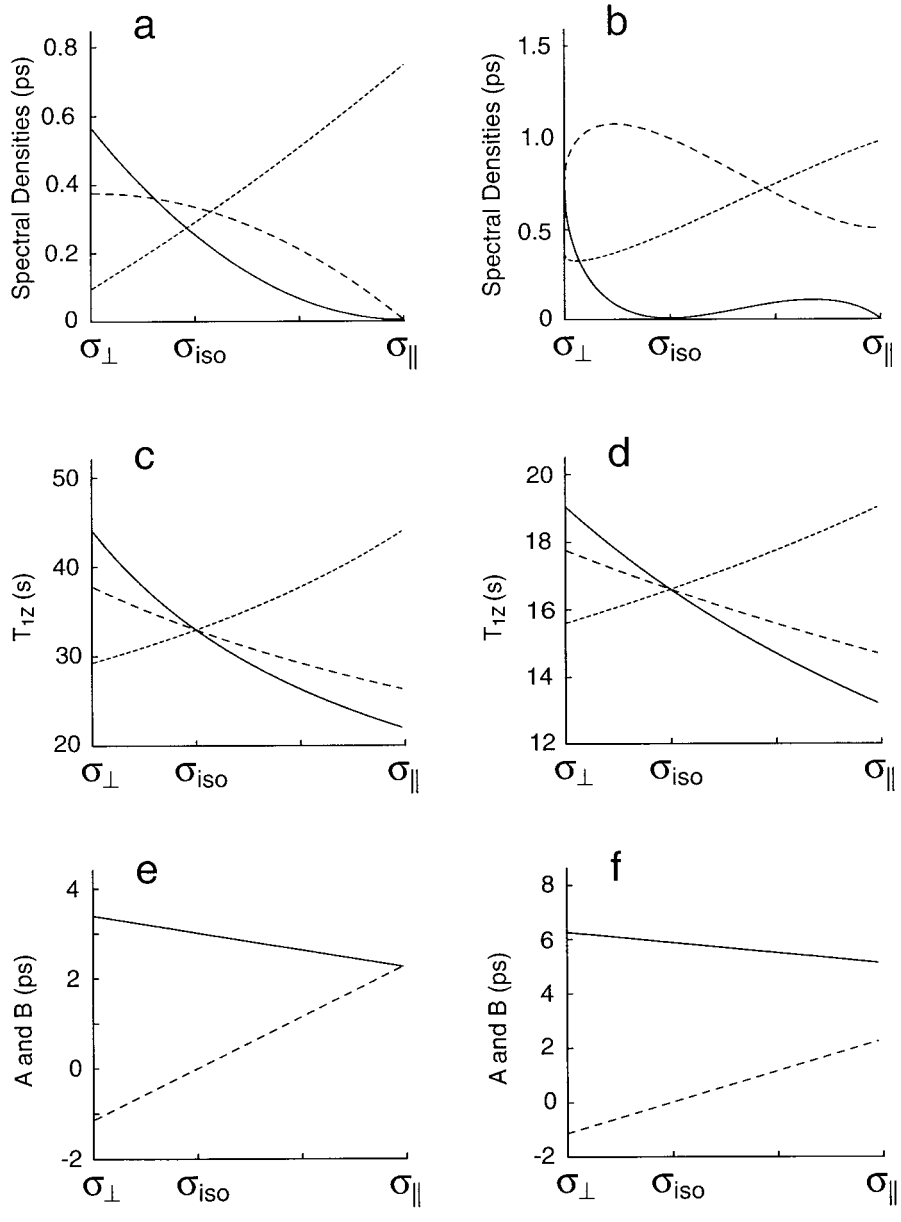

FIG. 1. Results of numerical calculations for two models of molecular motion. The first column (a, c, e) shows results for a five-site jump model where the angle between the ^{13}C–^{1}H vector and the motional axis, β_{PM}, is 90°. In the second column (b, d, f) a three-site jump model is used with $\beta_{PM} = 70.5°$, appropriate to a methyl group. The jump rate is 1.0×10^{11} s^{-1} for both models. (a, b) The static spectral densities, $J_0(0)$ (solid), $J_1(0)$ (dashed), and $J_2(0)$ (dotted), allow these models to be easily distinguished. For the three-site model (a) only the spectral densities for $0° \leq \beta_{CR} < 90°$ are shown. (c, d) T_{1Z} anisotropies for spinning angles of 0° (solid), 35° (dotted), and 90° (dashed) for the two models are very similar. (e, f) Linear combinations of spectral densities, *A* (solid) and *B* (dotted), for the two models are more distinct.

Deuteron experiments were performed at a Larmor frequency of 46.06 MHz. A 90° pulse length of 1.6 μs was used. An inversion recovery pulse sequence with quadrupole echo detection was used to measure T_{1Z}. The relaxation delays were 0.05, 0.1, 0.2, 0.5, 1, 2, 5, and 10 s. A delay of 8 s was used between scans. For the T_{1Q} experiments, quadrupole order was created using the Broadband Jeener–Broekaert (*20*) pulse sequence with an excitation delay $5\tau = 27.5$ μs. The relaxation delays were 0.05, 0.1, 0.2, 0.5, 1, 2, 8, and 16 s, and the recycle time was 16 s. The horns of the ferrocene powder pattern are intrinsically very sharp because T_2 is long. Thus, an unusually long echo delay of 100 μs was required to avoid distortion of the quadrupolar echo by the virtual FID.

Data analysis was performed on a Silicon Graphics O2 workstation with customized PV-WAVE software. Relaxation times of each point on the powder lineshape were determined by a two-parameter nonlinear least-squares fit to the experimental data.

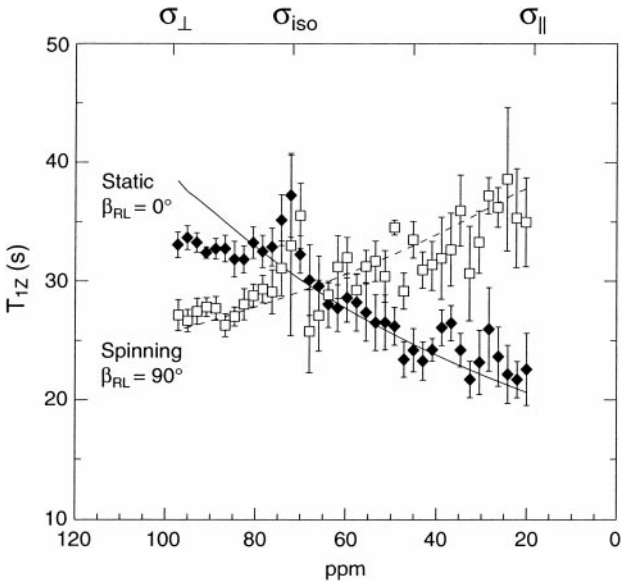

FIG. 2. Measured and calculated ^{13}C T_{1Z} anisotropies for ferrocene. The filled diamonds are the measured relaxation times for a static sample. Measured relaxation times for a sample spinning at 90° with respect to the field are indicated with open squares. The width of the powder pattern of the spinning sample was scaled by a factor of −2 before relaxation times were measured. The solid line is the calculated anisotropy for the static sample. The calculated anisotropy for the spinning sample is indicated with a dashed line. Experimental errors (±1 standard deviation) were determined by the fitting procedure. The rates used for the calculations are $1.1 \pm 0.1 \times 10^{11}$ s^{-1} for the fivefold all-site jump model, $1.5 \pm 0.1 \times 10^{11}$ s^{-1} for the five-site model with jumps only to neighboring sites, and $1.4 \pm 0.1 \times 10^{11}$ s^{-1} for rotational diffusion. These rates give the best fit of the linear combinations of spectral densities. (See text for details.)

RESULTS

Carbon Relaxation Time Anisotropies

For ferrocene, measurement of anisotropic relaxation times is straightforward because only one chemically distinct carbon is present in the molecule. However, in spinning samples, one must be careful to compare relaxation times of identical crystallite orientations, not measured chemical shift. Since spinning at 90° scales the powder pattern by a factor of −1/2, the width of the experimental OMAS spectrum was scaled by a factor of −2 to facilitate comparison with the static spectrum. The experimental T_{1Z} anisotropies plotted in Fig. 2 show the expected dependence on spinning angle, (β_{RL}).

For the static sample, relaxation times are longest at the $\sigma = \sigma_\perp$ edge. When the sample is spun at $\beta_{RL} = 90°$ the anisotropy is reversed, with the longest relaxation times on the shoulder ($\sigma = \sigma_\parallel$) of the powder pattern.

For carbons with directly bonded protons, the dominant relaxation mechanism is usually the dipolar interaction with ^1H nuclei. In order to ensure that the CSA relaxation mechanism can be safely ignored in ferrocene, the relaxation time due to CSA alone was estimated from the width of the static powder pattern. If this value of T_{1Z} is much longer than the measured relaxation rates then the assumption that the dipolar interaction dominates ^{13}C relaxation in ferrocene is justified. For an axially symmetric chemical shielding tensor the relaxation rate due to chemical shift anisotropy is given by (*21*)

$$R_{1Z} = \frac{1}{15}\,\gamma^2 B_0^2(\sigma_\parallel - \sigma_\perp)^2\,\frac{2\tau_c}{1+\omega^2\tau_c^2}. \qquad [21]$$

For our experiments, $\gamma B_0 = 2\pi \times 75.46 \times 10^6$ s^{-1}. At room temperature, the width of the ferrocene powder pattern is 80 ± 1 ppm. This lineshape is narrowed by a factor of 2 due to fast rotation about the molecule's C_{5V} symmetry axis; thus, $\sigma_\parallel - \sigma_\perp = 160$ ppm. The correlation time is estimated to be five times the largest calculated dipolar spectral density, 8×10^{-13} s at the $\beta_{CR} = 0°$ edge of the static powder pattern. Substitution of these values into Eq. [21] yields a relaxation rate of 3.1×10^{-3} s. The corresponding spin–lattice relaxation time is 330 s, significantly longer than the longest measured relaxation time of 40 s. For other orientations, the estimated CSA relaxation times are even longer. Thus, chemical shift mechanism makes a negligible contribution to the relaxation ferrocene at room temperature.

For ferrocene the experimental anisotropies of *A* and *B* are presented in Fig. 3. These are shown to agree well with the dipolar relaxation calculations.

The curves for *A* and *B* nearly overlap at the parallel edge of the powder lineshape confirming that the angle between the

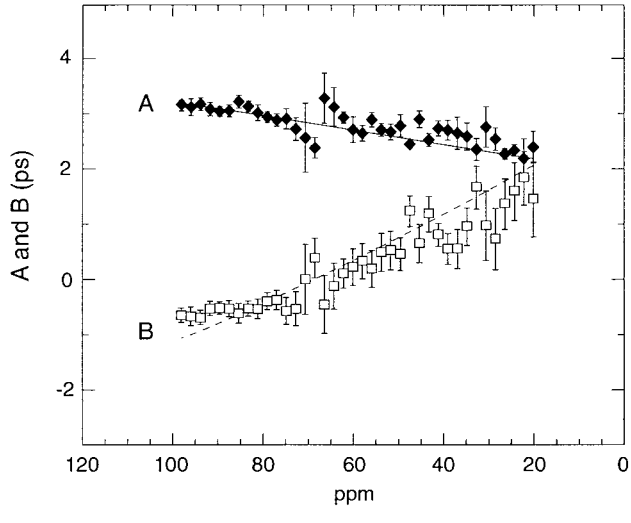

FIG. 3. For ferrocene, experimental (symbols) and best fit values (lines) of the linear combinations of spectral densities *A* and *B* determined from the static and spinning ^{13}C T_{1Z} anisotropies. The rates used for the calculations are $1.1 \pm 0.1 \times 10^{11}$ s^{-1} for the fivefold all-site jump model and $1.5 \pm 0.1 \times 10^{11}$ s^{-1} for the five-site model with jumps only to neighboring sites. The diffusion constant for the rotational diffusion model is $1.4 \pm 0.1 \times 10^{11}$ s^{-1}. The convergence of *A* and *B* at the $\sigma_\parallel$ edge of the powder pattern indicates that the angle between the ^{13}C–^1H vector and the axis of motion is close to 90°.

^{13}C–^{1}H vector and the motional axis of ferrocene is very close to 90°. Neutron diffraction studies (*22*) have determined that the C–H vectors are displaced out of the plane of the cyclopentadienyl rings, toward the iron atom, by about 1.6°. Due to uncertainty in the data, this deviation is too small to be measured accurately by NMR.

In a sense, the molecular geometry of ferrocene is unfortunate. For $\beta_{PM} = 90°$ the expression for $J_m(\omega)$ (Eq. [11]) simplifies further because $d^{(2)}_{\pm 20}(90°) = 3/8$, $d^{(2)}_{\pm 10}(90°) = 0$, and $d^{(2)}_{00}(90°) = -1/2$. Thus, the $b = 1$ terms vanish. The $b = 0$ terms are ignored because $\Gamma_{0,0}$ does not decay with time. Furthermore, for axial motion in the extreme narrowing limit, $\Gamma_{2,2}$ is simply a constant, inversely proportional to the motional rate or diffusion coefficient. The spectral densities for ferrocene are

$$J_m(0) = \frac{3}{8}\frac{1}{ck}\sum_a |d^{(2)}_{am}(\beta_{RL})|^2\{|d^{(2)}_{2a}(\beta_{CR})|^2 + |d^{(2)}_{2a}(\beta_{CR})|^2\}, \quad [22]$$

where k is the jump rate and c is a number that depends on the motional model. For a five-site model with jumps to all sites allowed, $c = 5$, if only jumps to nearest neighbor sites occur, $c = 4\sin^2(2\pi/5) \approx 3.62$, and for diffusive motion $c = 4$. Under these conditions, the spectral densities for different models and rates differ only by the constant factor $1/ck$. As a result, for this geometry, the subtleties of the motional trajectory cannot be differentiated. For ferrocene, the best fit rate for each model was determined by manually varying the rates used for the calculations so as to minimize χ^2 of the calculated and measured A and B anisotropies.

If a ^{13}C–^{1}H bond length of 1.08 Å is used ($\omega_D = 1.51 \times 10^5$ rad/s) then the A and B anisotropies are best fit with a jump rate of $k = 1.1 \pm 0.1 \times 10^{11}$ s^{-1} for the five-site model with jumps to all sites allowed. The best-fit rates for the other models were found to be in agreement with Eq. [22]. Thus, the best-fit rate for the five-site model with jumps to neighboring sites is $1.5 \pm 0.1 \times 10^{11}$ s^{-1} and for diffusive motion the diffusion constant is $1.4 \pm 0.1 \times 10^{11}$ s^{-1}. These results are in reasonable agreement with neutron scattering measurements (*23*). Assuming a five-site nearest neighbor jump model, the neutron data give a rate of $1.1 \pm 0.2 \times 10^{11}$ s^{-1}, whereas the experimental NMR data yield a best fit value of $1.5 \pm 0.1 \times 10^{11}$ s^{-1}.

The ^{13}C–^{1}H bond length of 1.08 Å was determined by requiring motional rates measured by carbon relaxation to agree with the deuteron rates presented later in this paper. Studies of the dynamics of benzene (*11*) show that correlation times for the protonated and deuterated molecule differ by only a few percent at room temperature. Since the structure and dynamics of ferrocene are similar to benzene's, isotope effects in ferrocene are unlikely to be significant compared to experimental uncertainties. The ferrocene bond length used, 1.08 Å, is larger than published values determined from neutron diffraction studies (*22, 24*). The values in these studies ranged from 0.903 to 1.056 Å at 298 K, depending on the refinement model used. The correction of the dipolar coupling constant resulting from the use of an appropriately vibrationally averaged bond length, instead of the equilibrium value, has been calculated (*11*) to be $(1.080/1.106)^3$ or −7%. When the ferrocene bond length used here is compared to the longest of the neutron diffraction values the vibrational correction is also about −7%. As noted in a preceding section of this paper, the vibrationally averaged bond length measured by neutron diffraction is expected to be closer to the equilibrium value than the length determined by the dipolar coupling strength.

The relaxation time of the ferrocene peak in a CPMAS experiment was measured to be $T_{1Z} = 32.0 \pm 0.4$ s. The relaxation of this peak displays no apparent multiexponential behavior. This is expected since, for five-site motion, the time-dependent part of the correlation function, $\Gamma_{b,b'}(t)$, is diagonal. As mentioned previously, a diagonal $\Gamma_{b,b'}(t)$ leads to relaxation times that do not depend on crystallite orientation for a sample spinning at the magic angle.

Deuteron Relaxation Time Anisotropies

The fact that, for relatively isolated ^{13}C–^{1,2}H pairs, the quadrupole and the dipolar interaction tensors have nearly the same orientation and orientational dependence means that deuteron relaxation time anisotropies offer additional, complementary information about the spectral densities in ferrocene. The measured deuteron T_{1Z} and T_{1Q} anisotropies, shown in Fig. 4, fit very well to the anisotropies calculated from simple five-fold axial motional models. Again, because of the molecular geometry of ferrocene, jump and diffusive motion could not be distinguished. The quadrupole coupling constant was assumed to be twice the motionally averaged value measured from the NMR spectrum. For motion with equiprobable jumps to all five sites the best fit rate is $1.06 \pm 0.01 \times 10^{11}$ s^{-1}. For a five-site nearest neighbor jump model, the best fit rate is $1.47 \pm 0.01 \times 10^{11}$ s^{-1}. For unrestricted rotational diffusion, the best fit diffusion constant is $1.33 \pm 0.01 \times 10^{11}$ s^{-1}. Within experimental error, these rates agree with those determined from ^{13}C relaxation. Since the calculated ^{13}C relaxation time anisotropies depend sensitively on the ^{13}C–^{1}H bond length, this agreement supports a ferrocene bond length of 1.08 Å.

An expression for the zero quantum spectral density, $J_0(0)$, is found by rearranging Eq. [20] for R_{1Z}, the Zeeman relaxation rate of ^{13}C under CPMAS conditions,

$$J_0(0) = \frac{R_{1Z}}{N\omega_D^2} - 2[J_1(0) + J_2(0)]. \quad [23]$$

The carbon relaxation rate measured under CPMAS conditions is independent of crystallite orientation, and the orientation dependence of the two spectral densities $J_1(0)$ and $J_2(0)$ can

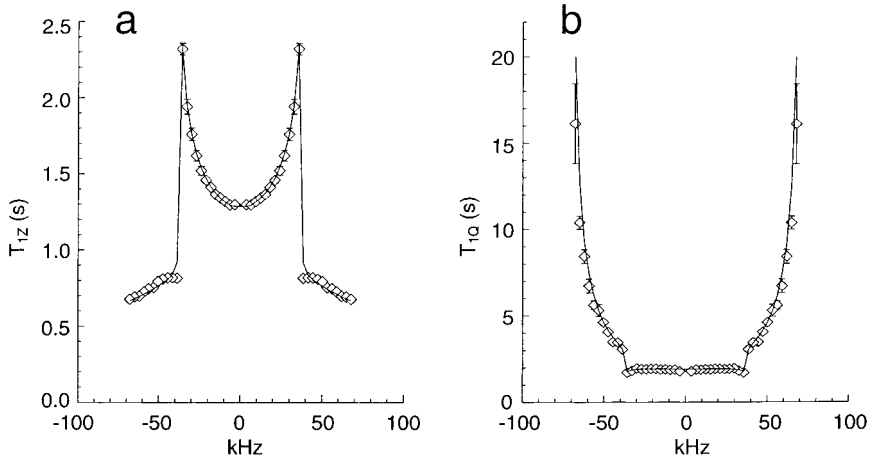

FIG. 4. Measured and best fit deuteron (a) T_{1Z} and (b) T_{1Q} anisotropies for ferrocene. Calculated anisotropies correspond to a five-site jump model with a jump rate of $1.06 \pm 0.01 \times 10^{11}$ s^{-1}, a five-site model with jumps to neighboring sites at a rate of $1.47 \pm 0.01 \times 10^{11}$ s^{-1}, or a free diffusion model with a diffusion constant of $1.33 \pm 0.01 \times 10^{11}$ s^{-1}. The molecular geometry of ferrocene prevents these models from being distinguished. Error bars representing the experimental errors determined by the fitting procedure are plotted along with the measured relaxation times. In some cases the error bars are smaller than the symbols.

be determined from relaxation measurements of deuteron R_{1Z} and R_{1Q}. Thus, Eq. [23] shows that, in the extreme narrowing limit, the orientation dependence of the zero quantum spectral density can be obtained by combining carbon and deuteron relaxation data. This method was used to perform the first experimental determination of $J_0(0)$ in a solid. As illustrated in Fig. 5, the experimental spectral densities closely match the simulated data.

The quadrupole coupling constant, χ, used in the deuteron relaxation calculations was twice that measured from the room temperature spectrum. This value is less than the rigid lattice coupling constant since averaging of the interaction due to vibrations and librations is implicitly included. However, the value of χ used in the calculations is appropriate because these motions are too fast to cause relaxation.

Substitution of the spectral densities (Eq. [22]) into the expressions for R_{1Z} (Eqs. [1] and [2]) shows that $R_{1Z}(^{13}\mathrm{C}) \propto \omega_D^2/k$ for carbon, and $R_{1Z}(^2\mathrm{H}) \propto \chi^2/k$ for deuterons. Since we require that the rate of motion, k, be the same for both carbon and deuteron relaxation, the ratio of the two rates is ω_D^2/χ^2. The quadrupole coupling constant has been determined; thus, an expression for the dipolar coupling constant can be written

$$\omega_D = \chi \sqrt{\frac{R_{1Z}(^{13}\mathrm{C})}{R_{1Z}(^2\mathrm{H})}}. \qquad [24]$$

This expression could be used to evaluate ω_D and hence, $\langle 1/r_{CH}^3 \rangle$. It also provides a means for estimating the uncertainty in the ^{13}C–^{1}H bond length. The average uncertainty in $R_{1Z}(^{13}\mathrm{C})$ is 7.7%. For the deuteron data the average uncertainty is 1.4%. We estimate that the value used for χ is within 1% of the correct value. Propagation of these errors through Eq. [23] leads to an uncertainty in ω_D of 4.0%. The ^{13}C–^{1}H bond length, $\langle 1/r_{CH}^3 \rangle^{-1/3}$, determined in this study is thus 1.08 ± 0.02 Å.

CONCLUSIONS

NMR spin–lattice relaxation time anisotropies provide valuable information about molecular dynamics. These relaxation times are linear combinations of the spectral density functions which describe the time dependence of local spin interactions. In order to rigorously test models of molecular motion, measurement of all relevant spectral densities is advantageous. A variety of carbon and deuteron relaxation time anisotropies were measured for ferrocene in an attempt to obtain as many linear combinations of the spectral densities as possible.

The ^{13}C results presented here demonstrate theoretical and experimental methods for obtaining the two linear combinations of the spectral densities responsible for ^{13}C dipolar relaxation. The method makes use of the observation that, in spinning samples, carbon T_{1Z} anisotropies depend on the orientation of the spinning axis. In the extreme narrowing limit, where the spectral densities are independent of frequency, these anisotropies are linear combinations of the static spectral densities with coefficients that depend on the spinning angle. Because of the functional dependence of these coefficients on the spinning angle, only two independent linear combinations of the static spectral densities can be determined.

These linear combinations, A and B, are sensitive to molecular geometry. In particular, the difference between A and B for $\beta_{CR} = 0°$ is correlated with the angle between the z-axes of the principal axis system and molecular frame. For ferrocene, where $\beta_{PM} = 90°$, similar models of motion (fivefold jumps to all sites, fivefold jumps to neighboring sites and rotational

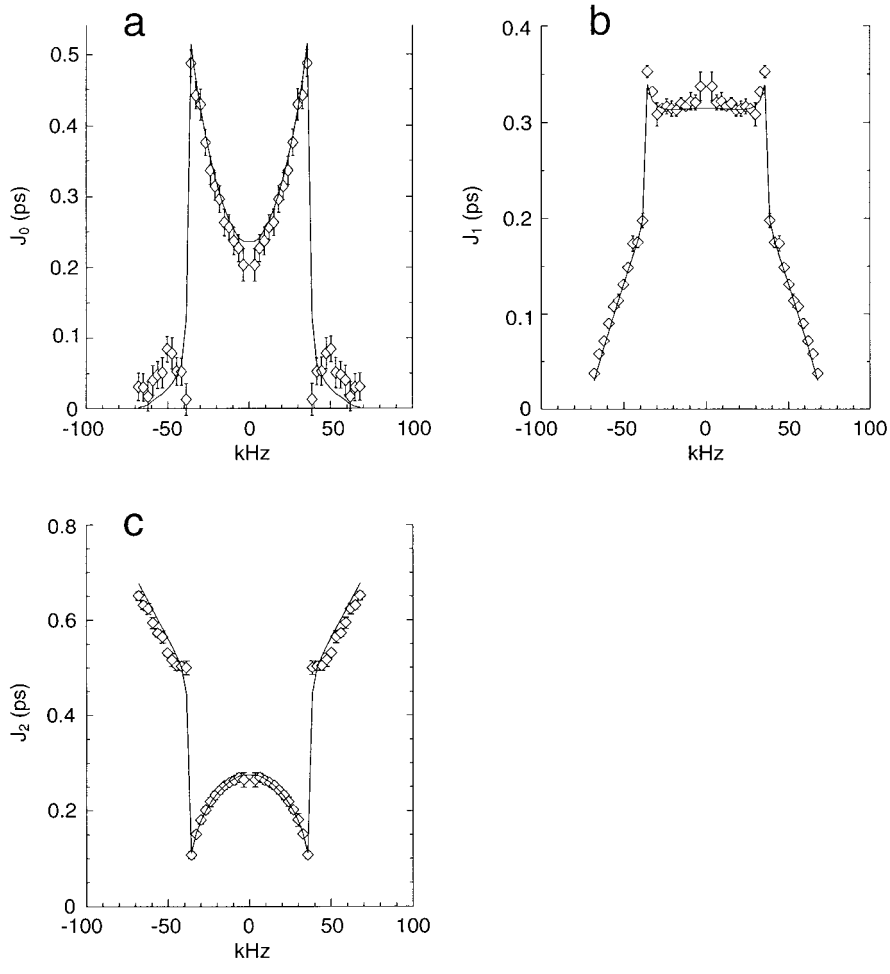

FIG. 5. The anisotropies of individual spectral densities (a) $J_0(0)$, (b) $J_1(0)$, and (c) $J_2(0)$ for ferrocene. $J_1(0)$ and $J_2(0)$ were determined from the deuteron T_{1Z} and T_{1Q} relaxation time anisotropies. The ^{13}C CPMAS T_{1Z} provided the additional linear combination of spectral densities needed to determine $J_0(0)$.

diffusion) are not distinguishable by measurement of A and B. This is a special case; for other molecular geometries, calculations show that these models are distinguishable. Thus, natural abundance ^{13}C relaxation time measurements can provide detailed motional information.

The measurement of the anisotropies of deuteron Zeeman and quadrupolar relaxation times, T_{1Z} and T_{1Q}, allow the determination of two spectral densities, $J_1(\omega_0)$ and $J_2(2\omega_0)$. Motional rates determined from these data are in good agreement with results of neutron scattering experiments (*23*). For fast uniaxial motional models, combining these results with carbon relaxation experiments provides the additional constraint necessary for the determination of a third spectral density, $J_0(0)$. This paper reports the first experimental measurement of the orientation dependence of $J_0(0)$. The combination of ^{13}C and ^{2}H relaxation data also allowed the determination of the ^{13}C–^{1}H dipolar coupling strength and, thus, the ^{13}C–^{1}H bond length.

This paper describes a method for obtaining information about molecular motion with a level of detail previously unavailable from natural abundance ^{13}C NMR. The overlap of anisotropic lineshapes hampers analysis of ^{13}C NMR spectra just as it does for other nuclear species. Resonances from chemically distinct deuterons can sometimes be measured with selectively deuterated samples. For carbon NMR, separation of powder patterns on the basis of isotropic chemical shift in a 2D spectrum can provide selectivity. When applied with care, 2D techniques should allow detailed motional information to be obtained for each chemically distinct carbon in complex molecules.

REFERENCES

1. G. L. Hoatson and R. L. Vold, *NMR Basic Prin. Prog.* **32,** 1 (1994).
2. J. Z. Hu, W. Wang, F. Liu, M. S. Solum, D. W. Alderman, R. J. Pugmire, and D. M. Grant, *J. Magn. Reson. A* **113,** 210 (1995).
3. L. Frydman, G. C. Chingas, Y. K. Lee, P. J. Grandinetti, M. A. Eastman, G. A. Barall, and A. Pines, *J. Chem. Phys.* **97,** 4800 (1992).
4. V. A. Daragan and K. H. Mayo, *Prog. NMR Spectros.* **31,** 63 (1997).

5. L. G. Werbelow and D. M. Grant, *Adv. Magn. Reson.* **9,** 189 (1977).
6. K. Elbayed and D. Canet, *Mol. Phys.* **68,** 1033 (1989).
7. P. Allard and T. Härd, *J. Magn. Reson.* **126,** 48 (1977).
8. D. Theimer and G. Bodenhausen, *Appl. Magn. Reson.* **3,** 1071 (1992).
9. D. A. Torchia and A. Szabo, *J. Magn. Reson.* **49,** 107 (1982).
10. R. R. Vold and R. L. Vold, *Adv. Magn. Optical Reson.* **16,** 85 (1991).
11. E. H. Hardy, R. Witt, A. Dölle, and M. D. Zeidler, *J. Magn. Reson.* **134,** 300 (1998).
12. E. R. Henry and A. Szabo, *J. Chem. Phys.* **82,** 4753 (1985).
13. S. Sýkora, J. Vogt, H. Bösiger, and P. Diehl, *J. Magn. Reson.* **36,** 53 (1979).
14. R. R. Ernst, G. Bodenhausen, and A. Wokaun, "Principles of Nuclear Magnetic Resonance in One and Two Dimensions," Oxford, New York (1987).
15. R. Tycko, G. Dabbagh, and P. A. Mirau, *J. Magn. Reson.* **85,** 265 (1989).
16. A. Bax, N. M. Szeverenyi, and G. E. Maciel, *J. Magn. Reson.* **52,** 147 (1983).
17. A. Bax, N. M. Szeverenyi, and G. E. Maciel, *J. Magn. Reson.* **55,** 494 (1983).
18. S. J. Varner, R. L. Vold, and G. L. Hoatson, *J. Magn. Reson. A* **123,** 72 (1996).
19. D. A. Torchia, *J. Magn. Reson.* **30,** 613 (1987).
20. G. L. Hoatson, *J. Magn. Reson.* **94,** 152 (1991).
21. T. C. Farrar and E. D. Becker, "Pulse and Fourier Transform NMR," Academic Press, New York (1971).
22. F. Takusagawa and T. F. Koetzle, *Acta Crystallogr.* **B35,** 1074 (1979).
23. A. B. Gardner, J. Howard, T. C. Waddington, R. M. Richardson, and J. Tomkinson, *Chem. Phys.* **57,** 453 (1981).
24. C. P. Brock and Y. Fu, *Acta Crystallogr.* **B53,** 928 (1997).